Journal of Solid State Chemistry **161,** 85–92 (2001)
doi:10.1006/jssc.2001.9284, available online at http://www.idealibrary.com on IDEAL®

Crystallization and Structural Characterization of Two Europium Molybdates, $Eu_4Mo_7O_{27}$ and $Eu_6Mo_{10}O_{39}$

H. Naruke[1] and T. Yamase

Chemical Resources Laboratory, Tokyo Institute of Technology, 4259 Nagatsuta, Midori-ku, Yokohama 226–8503, Japan
E-mail: hnaruke@res.titech.ac.jp

Received April 24, 2001; in revised form June 14, 2001; accepted June 20, 2001; published online August 22, 2001

Crystals of two new europium molybdates, $Eu_4Mo_7O_{27}$ and $Eu_6Mo_{10}O_{39}$, were grown in a melt of $Eu_2O_3 \cdot 6.1$–$6.5MoO_3$ obtained by thermal decomposition of $[Eu_2(H_2O)_{12}Mo_8O_{27}] \cdot 6H_2O$ or firing of the $Eu_2O_3 + 8MoO_3$ mixture at 800°C for 2h in air. Repeated uses of reaction containers are effective in the crystallization. $Eu_4Mo_7O_{27}$ crystallized in monoclinic, $C2/c$ (No. 15), $a = 23.031(1)$, $b = 14.720(1)$, $c = 14.4097(7)$ Å, $\beta = 105.174(2)°$, $V = 4714.8(4)$ Å^3, $Z = 8$, $R_1 = 0.035$, and $wR_2 = 0.064$. $Eu_4Mo_7O_{27}$ is a layer compound consisting of $\{MoO_4\}$- and $\{Mo_3O_{11}\}$-containing layers parallel to the bc plane and interstitial Eu atoms. $Eu_6Mo_{10}O_{39}$ crystallized in monoclinic, $C2/c$ (No. 15), $a = 12.3008(5)$, $b = 19.6596(9)$, and $c = 13.7691(4)$ Å, $\beta = 100.8934(9)°$, $V = 3269.8(2)$ Å^3, $Z = 4$, $R_1 = 0.036$, and $wR_2 = 0.101$. The structure of $Eu_6Mo_{10}O_{39}$ is constructed of three-dimensionally arranged $\{MoO_4\}$ and $\{Mo_2O_7\}$ groups and Eu atoms, being closely related to the structure of $Ce_6Mo_{10}O_{39}$. In both compounds, Eu atoms achieve seven- or eight-fold coordination by O atoms (< 2.7 Å), and two EuO_n polyhedra share their edges or faces with a short Eu···Eu separations ranging from 3.6297(8) to 3.7168(6) Å.

Key Words: **rare-earth molybdates; europium molybdates; polyoxomolybdates; thermal decomposition; crystal structures.**

INTRODUCTION

Phase equilibria and crystal structures of a R_2O_3–MoO_3 (R = rare earths) system have long been explored and several compounds attract interests as inorganic materials (1). Since the discovery (2) of ferroelectric and ferroelastic properties of a series of $R_2(MoO_4)_3$ (especially for $Gd_2(MoO_4)_3$), much attention has been paid to their preparation method, crystal growth, polymorphology, phase transition, and application to optoelectronic devices (1). R_2MoO_6-based compounds are also of interest because of their potent catalytic activities (3). Recent topics on rare-earth molybdates are ionic conduction behavior of $La_2Mo_2O_9$ and $R_2(MoO_4)_3$, which exhibit fast oxide-ion (4, 5) and trivalent ion (R^{3+}) (6) conductions, respectively. In contrast to these well-characterized materials, information on other rare-earth molybdates is rather poor. Of the rare-earth molybdates with R_2O_3:MoO_3 = 1:6, 1:4, 1:3, 1:2, 2:1, 3:1, 3:10, 7:8, and 9:4 found in the phase equilibria (7), most of the structural studies have concentrated on $R_2(MoO_4)_3$ (1:3), R_2MoO_6 (1:1), and their polymorphs (1, 3). In particular, very little is known about the Eu_2O_3–MoO_3 system (7).

The present study describes the crystal structures of two novel europium molybdates, $Eu_4Mo_7O_{27}$ (2:7) and $Eu_6Mo_{10}O_{39}$ (3:10), in which the former is a first observation in the R_2O_3–MoO_3 system. The latter stoichiometry has been reported as $Ce_6Mo_{10}O_{39}$ (8), a structure of which is different but closely related to $Eu_6Mo_{10}O_{39}$. Both europium molybdates were found in a melt of a 800°C-decomposed polyoxomolybdoeuropate, $[Eu_2(H_2O)_{12}Mo_8O_{27}] \cdot 6H_2O$ (9), which consists of an inifinite γ-octamolybdate polymer $\{(Mo_8O_{27})^{6-}\}_\infty$ attached by hexahydrated $[Eu(H_2O)_6]^{3+}$ cations and lattice water molecules. It was found that the firing of a mixture of Eu_2O_3 and MoO_3 in a 1:8 molar ratio at 800°C also produced $Eu_4Mo_7O_{27}$ and $Eu_6Mo_{10}O_{39}$. However, these preparation methods are not always successful, frequently yielding no crystals in the melt. We also describe and discuss the formation and crystallization conditions of the two compounds.

EXPERIMENTAL

Materials and Reactions

All chemicals were of analytical grade and used without further purification. The $[Eu_2(H_2O)_{12}Mo_8O_{27}] \cdot 6H_2O$ powder was synthesized according to the literature (9), and ground in an agate mortar. The firing of samples in air was carried out using a temperature-controlled electric furnace with a horizontally arranged cylindrical heater (diameter, 60 mm; length, 300 mm) and an inner quartz tube (diameter,

[1] To whom correspondence should be addressed. Fax + 81-(0)45-924-5276.

0022-4596/01 $35.00

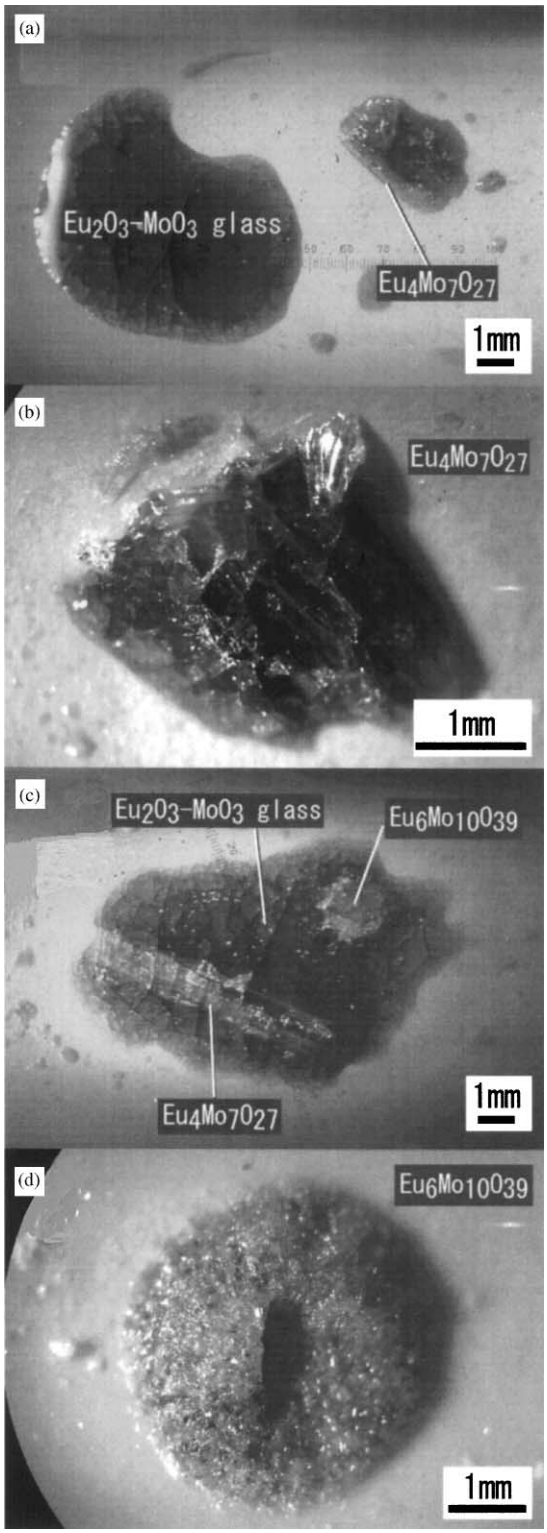

FIG. 1. Microscopic images of $Eu_4Mo_7O_{27}$ and $Eu_6Mo_{10}O_{39}$ crystals obtained by firing (a) $[Eu_2(H_2O)_{12}Mo_8O_{27}]\cdot 6H_2O$, (b) $Eu_4Mo_7O_{27} + [Eu_2(H_2O)_{12}Mo_8O_{27}]\cdot 6H_2O$, (c) $Eu_2O_3 + 8MoO_3$, and (d) $Eu_6Mo_{10}O_{39} + [Eu_2(H_2O)_{12}Mo_8O_{27}]\cdot 6H_2O$ at 800°C for 2 h. The crystals in (a) and (c) were obtained by reusing the same alumina containers (see text).

30 mm; length, 860 mm). Both ends of the tube were closed with rubber caps when heating. The samples were heated in a boat-shaped alumina container (width, 10 mm; height, 10 mm; length, 70 mm). The sample position in the furnace was carefully selected so that the temperature error was within ± 5°C.

Preparation of $Eu_4Mo_7O_{27}$

Placed in the boat, the $[Eu_2(H_2O)_{12}Mo_8O_{27}]\cdot 6H_2O$ was inserted in the 800°C-preheated furnace and kept at

TABLE 1
Crystallographic Data and Results for the Structural Analyses

Compound	$Eu_4Mo_7O_{27}$	$Eu_6Mo_{10}O_{39}$
Formula weight	1171.40	2495.14
Temperature (K)	173	173
X-ray source	Mo$K\alpha$ (0.71069 Å)	Mo$K\alpha$ (0.71069 Å)
Crystal system	Monoclinic	Monoclinic
Space group (No.)	$C2/c$ (No. 15)	$C2/c$ (No. 15)
Unit cell dimensions	$a = 23.031(1)$ Å	$a = 12.3008(5)$ Å
	$b = 14.720(1)$ Å	$b = 19.6596(9)$ Å
	$c = 14.4097(7)$ Å	$c = 13.7691(4)$ Å
	$\beta = 105.174(2)$°	$\beta = 100.8934(9)$°
Volume	4714.8(4) Å^3	3269.8(2) Å^3
Z	8	4
D_{calc}	4.822 g cm^{-3}	5.068 g cm^{-3}
μ(Mo$K\alpha$)	141.35 cm^{-1}	150.97 cm^{-1}
F(000)	6096	4440
Crystal size (mm^3)	$0.30\times0.08\times0.10$	$0.10\times0.10\times0.08$
Crystal color and habit	colorless, block	colorless, block
Diffractometer	Rigaku RAXIS-RAPID imaging plate	Rigaku RAXIS-RAPID imaging plate
Data collection	Oscillation method	Oscillation method
Oscillation range	$\phi = 0°$, $\chi = 45°$, $\omega = 130°$–$190°$, $\phi = 180°$, $\chi = 45°$, $\omega = 0°$–$160°$	$\phi = 0°$, $\chi = 45°$, $\omega = 130°$–$190°$, $\phi = 180°$, $\chi = 45°$, $\omega = 0°$–$160°$
Oscillation width	$\Delta\omega = 5°$	$\Delta\omega = 5°$
Exposure	1 min/°	1 min/°
$2\theta_{max}$	55°	55°
Reflections		
Total	21822	15542
Unique (R_{int})	5615 (0.080)	3733 (0.074)
Observed	4467 ($I > 2\sigma(I)$)	3309 ($I > 2\sigma(I)$)
Transmission factor	0.1380–0.3228	01086–0.3259
Minimizing quantity on LS	$\sum w(F_o^2 - F_c^2)^2$	$\sum w(F_o^2 - F_c^2)^2$
No. of variables	343	249
R_1^a, wR_2^b	0.035, 0.064	0.036, 0.101
Maximum shift/error	0.002	0.001
Goodness of fit	1.86	1.12
$\Delta\rho_{max}$	1.74 e$^-$ Å^{-3} (1.74 Å from Eu(3))	1.88 e$^-$ Å^{-3} (0.92 Å from Eu(1))
$\Delta\rho_{min}$	-7.23 e$^-$ Å^{-3} (0.57 Å from Eu(4))	-5.78 e$^-$ Å^{-3} (0.78 Å from Eu(3))

[a] $R_1 = \sum \|F_o| - |F_c\| / \sum |F_o|$ for $I > 2\sigma(I)$.
[b] $wR_2 = \{\sum[w(F_o^2 - F_c^2)^2] / \sum[w(F_o^2)^2]\}^{1/2}$, where $w = [\sigma_c^2(F_o^2) + p(\mathrm{Max}(F_o^2, 0) + 2F_c^2)/3\}^2]^{-1}$, $p = 0.01$ for $Eu_4Mo_7O_{27}$, $p = 0.05$ for $Eu_6Mo_{10}O_{39}$.

TABLE 2
Positional and Displacement Parameters

Atom	x	y	z	U_{eq}(Å^2)	Atom	x	y	z	U_{eq}(Å^2)
		$Eu_4Mo_7O_{27}$					$Eu_6Mo_{10}O_{39}$		
Eu(1)	0.11468(1)	0.94183(3)	0.14515(2)	0.00779(9)	Eu(1)	0.62533(3)	0.65578(2)	0.64568(3)	0.0083(1)
Eu(2)	0.62224(1)	0.80716(3)	− 0.06347(2)	0.00758(9)	Eu(2)	0.41330(3)	0.64879(2)	0.41452(3)	0.0085(1)
Eu(3)	0.61104(1)	0.94064(3)	0.14556(2)	0.00774(9)	Eu(3)	0.41260(3)	0.94262(2)	0.91610(3)	0.0118(1)
Eu(4)	0.38039(2)	0.69446(3)	0.06576(2)	0.00851(9)	Mo(1)	0.91343(7)	0.65447(3)	0.83972(5)	0.0120(2)
Mo(1)	0.25540(3)	0.80150(5)	0.16578(4)	0.0080(1)	Mo(2)	0.60343(5)	0.78370(4)	0.86136(4)	0.0084(2)
Mo(2)	0.23021(2)	0.88062(5)	0.38732(4)	0.0088(1)	Mo(3)	0.81461(6)	0.50026(4)	0.63939(5)	0.0100(2)
Mo(3)	0.23507(3)	0.59812(5)	0.29796(4)	0.0087(1)	Mo(4)	0.59434(6)	0.52063(4)	0.86154(5)	0.0091(2)
Mo(4)	0.56998(3)	1.05418(5)	− 0.10035(4)	0.0080(1)	Mo(5)	0.80586(6)	0.80898(4)	0.61804(5)	0.0110(2)
Mo(5)	− 0.06871(3)	0.95043(5)	0.10161(4)	0.0081(1)	O(1)	0.8739(5)	0.4967(3)	0.7656(4)	0.022(2)
Mo(6)	0.06123(2)	0.69609(5)	0.14481(4)	0.0079(1)	O(2)	0.9209(5)	0.4992(3)	0.5664(4)	0.019(2)
Mo(7)	0.56198(3)	0.69459(5)	0.14559(4)	0.0084(1)	O(3)	0.8944(5)	0.8305(3)	0.5319(4)	0.012(1)
O(1)	0.5794(2)	0.9753(4)	0.2875(3)	0.017(1)	O(4)	1.0000	0.6238(4)	0.7500	0.020(2)
O(2)	0.5895(2)	0.7851(4)	0.0862(3)	0.014(1)	O(5)	0.7719(5)	0.6477(3)	0.7986(5)	0.016(2)
O(3)	0.5899(2)	0.9548(4)	− 0.0260(3)	0.010(1)	O(6)	0.6040(5)	0.5560(3)	0.7439(4)	0.017(1)
O(4)	0.6009(2)	0.7924(4)	− 0.2347(3)	0.022(2)	O(7)	0.5445(4)	0.7209(3)	0.9306(4)	0.014(1)
O(5)	0.6001(2)	0.6536(4)	− 0.0594(4)	0.015(1)	O(8)	0.7289(5)	0.4952(3)	0.9150(4)	0.021(2)
O(6)	0.1994(2)	0.8794(4)	0.2573(3)	0.012(1)	O(9)	0.6077(5)	0.7513(3)	0.7411(4)	0.015(1)
O(7)	0.3852(2)	0.8492(4)	0.0606(4)	0.015(1)	O(10)	0.5163(5)	0.5533(3)	0.3595(4)	0.014(1)
O(8)	0.3992(2)	0.7004(5)	0.2331(4)	0.026(2)	O(11)	0.4578(5)	0.5850(3)	0.5647(4)	0.014(1)
O(9)	0.0745(2)	1.0880(4)	0.1022(4)	0.019(1)	O(12)	0.7500(5)	0.5777(3)	0.6094(4)	0.019(2)
O(10)	0.0870(2)	0.9738(5)	0.2904(3)	0.022(2)	O(13)	0.7853(5)	0.7217(3)	0.6232(4)	0.018(2)
O(11)	0.0863(2)	0.7872(4)	0.0819(3)	0.014(1)	O(14)	0.5348(5)	0.8623(3)	0.8551(4)	0.015(1)
O(12)	0.1951(2)	1.0475(4)	0.1570(4)	0.018(1)	O(15)	0.4464(5)	0.7616(4)	0.3664(5)	0.028(2)
O(13)	0.0079(2)	0.9337(4)	0.1208(4)	0.021(2)	O(16)	0.2400(5)	0.7018(3)	0.4185(4)	0.017(1)
O(14)	0.2455(2)	0.7164(4)	0.2600(3)	0.017(1)	O(17)	0.3596(7)	0.6606(3)	0.2349(5)	0.032(2)
O(15)	0.7040(2)	0.7152(4)	− 0.0661(4)	0.016(1)	O(18)	0.2810(5)	0.5655(3)	0.3874(5)	0.023(2)
O(16)	0.6955(2)	0.9029(4)	− 0.1156(4)	0.018(1)	O(19)	0.6778(6)	0.8449(3)	0.5751(6)	0.026(2)
O(17)	0.5158(2)	0.7978(4)	− 0.1290(4)	0.020(1)	O(20)	0.9533(6)	0.6090(4)	0.9468(4)	0.028(2)
O(18)	0.6885(2)	0.8738(4)	0.0812(3)	0.012(1)					
O(19)	0.5048(2)	0.9174(4)	0.1113(3)	0.017(1)					
O(20)	0.5770(2)	1.0892(4)	0.1031(3)	0.019(1)					
O(21)	0.4847(2)	0.7069(4)	0.1294(4)	0.021(1)					
O(22)	0.6957(2)	1.0392(4)	0.1977(4)	0.019(1)					
O(23)	0.6875(2)	0.8764(4)	0.2856(4)	0.017(1)					
O(24)	0.2857(2)	0.7282(4)	0.0975(3)	0.014(1)					
O(25)	0.1944(2)	0.8493(4)	0.0782(3)	0.015(1)					
O(26)	0.0931(1)	0.9506(4)	− 0.0242(3)	0.010(1)					
O(27)	0.2052(2)	0.9763(4)	0.4308(4)	0.022(2)					

800°C for 2h after a recovery of the temperature. The sample was then quenched by exposure to ambient temperature. Colorless crystals of $Eu_4Mo_7O_{27}$ (often together with $Eu_6Mo_{10}O_{39}$) were formed in a gray-brown glassy melt of Eu_2O_3–MoO_3. However, the crystallization of $Eu_4Mo_7O_{27}$ was not always successful: one could find no crystals in the melt especially when the virgin alumina container was used. We found that repeated uses of the same container were effective in improving the crystallization properties. Figure 1a shows a photograph of $Eu_4Mo_7O_{27}$ obtained when the boat was reused three times. When the container was reused, the previous sample was removed from the container only mechanically, without further washing or chemical treatment. A firing (800°C, 2h) of the $Eu_4Mo_7O_{27}$ obtained as seed crystals covered with $[Eu_2(H_2O)_{12}Mo_8O_{27}]\cdot 6H_2O$ powders (20 mg) yielded well-formed large $Eu_4Mo_7O_{27}$ crystals (Fig. 1b). It should be noted that the addition of too much $[Eu_2(H_2O)_{12}Mo_8O_{27}]\cdot 6H_2O$ resulted in a dissolution of the seed crystals to the melt.

We found that heating a Eu_2O_3:$MoO_3 = 1{:}8$ mixture (same Eu:Mo ratio as $[Eu_2(H_2O)_{12}Mo_8O_{27}]\cdot 6H_2O$) under the same conditions yielded $Eu_4Mo_7O_{27}$ crystals in a gray-brown melt of Eu_2O_3–MoO_3. Also in this case, repeated uses of the same alumina container were effective in the crystallization. Figure 1c shows a $Eu_4Mo_7O_{27}$ crystal (together with $Eu_6Mo_{10}O_{39}$) formed in a container that was reused five times. IR spectrum: 977.7m, 950.7s, 939.2s(sh),

TABLE 3
Selected Interatomic Distances (Å)

$Eu_4Mo_7O_{27}$						$Eu_6Mo_{10}O_{39}$					
Eu(1)	O(9)	2.359(6)	Mo(1)	$O(23)^{ii}$	1.719(5)	Eu(1)	O(12)	2.290(6)	Mo(1)	O(20)	1.715(6)
	O(26)	2.364(4)		O(24)	1.726(5)		O(9)	2.326(5)		$O(15)^{vii}$	1.721(7)
	O(6)	2.369(5)		O(25)	1.769(5)		O(13)	2.424(6)		O(5)	1.731(7)
	O(10)	2.389(5)		O(14)	1.904(5)		O(6)	2.425(6)		O(4)	1.876(3)
	O(12)	2.391(5)		O(6)	2.368(5)		$O(3)^{i}$	2.426(5)	Mo(2)	$O(16)^{vii}$	1.739(6)
	O(13)	2.394(5)	Mo(2)	O(27)	1.702(6)		O(5)	2.504(6)		O(14)	1.755(6)
	O(11)	2.475(6)		$O(15)^{iii}$	1.737(6)		$O(7)^{ii}$	2.505(6)		O(9)	1.784(5)
Eu(2)	O(5)	2.320(6)		$O(18)^{ii}$	1.811(4)		O(11)	2.560(6)		O(7)	1.794(6)
	O(15)	2.327(5)		O(6)	1.821(4)	Eu(2)	O(18)	2.289(6)	Mo(3)	O(12)	1.731(6)
	O(17)	2.389(5)	Mo(3)	$O(22)^{iv}$	1.724(5)		O(15)	2.372(7)		$O(18)^{viii}$	1.740(7)
	O(4)	2.396(5)		$O(16)^{iii}$	1.725(4)		$O(3)^{i}$	2.376(6)		O(1)	1.755(6)
	O(3)	2.404(5)		$O(12)^{v}$	1.736(5)		O(16)	2.383(6)		O(2)	1.794(6)
	O(18)	2.443(5)		O(14)	1.860(6)		O(11)	2.391(5)	Mo(4)	$O(10)^{ix}$	1.739(6)
	O(16)	2.462(5)	Mo(4)	$O(19)^{vi}$	1.740(5)		O(17)	2.447(7)		O(8)	1.752(7)
	O(2)	2.486(4)		$O(1)^{vii}$	1.741(5)		O(10)	2.463(6)		O(6)	1.787(5)
Eu(3)	O(20)	2.350(6)		$O(7)^{vi}$	1.763(5)		$O(7)^{ii}$	2.532(6)		$O(11)^{ii}$	1.814(6)
	O(22)	2.389(5)		O(3)	1.800(5)	Eu(3)	$O(19)^{ii}$	2.235(6)	Mo(5)	O(19)	1.725(7)
	O(19)	2.389(5)	Mo(5)	O(13)	1.731(5)		$O(1)^{iii}$	2.297(6)		$O(17)^{vii}$	1.727(7)
	O(1)	2.399(4)		$O(5)^{i}$	1.735(6)		$O(2)^{iv}$	2.302(6)		O(13)	1.738(6)
	O(3)	2.400(5)		$O(10)^{viii}$	1.749(5)		$O(2)^{v}$	2.349(6)		O(3)	1.806(5)
	O(18)	2.424(4)		$O(26)^{ix}$	1.831(5)		O(14)	2.436(6)			
	O(2)	2.450(6)	Mo (6)	$O(17)^{i}$	1.730(5)		$O(20)^{vi}$	2.477(6)	Eu(1)	Eu(2)	3.7168(6)
	O(23)	2.491(5)		$O(4)^{iii}$	1.746(5)		$O(8)^{iii}$	2.483(6)	Eu(3)	$Eu(3)^{x}$	3.6297(8)
Eu(4)	O(7)	2.282(6)		$O(20)^{iv}$	1.755(6)						
	O(8)	2.337(5)		O(11)	1.797(5)						
	$O(26)^{i}$	2.341(5)	Mo(7)	$O(9)^{x}$	1.741(6)						
	O(21)	2.344(5)		O(21)	1.742(5)						
	O(24)	2.395(4)		$O(8)^{ii}$	1.745(5)						
	$O(25)^{i}$	2.412(5)		O(2)	1.786(5)						
	$O(11)^{i}$	2.458(4)									
			Eu(1)	$Eu(4)^{i}$	3.6681(5)						
			Eu(2)	Eu(3)	3.6615(5)						

Note. Symmetry codes for $Eu_4Mo_7O_{27}$: (i) $\frac{1}{2}-x, \frac{3}{2}-y, -z$; (ii) $1-x, y, \frac{1}{2}-z$; (iii) $-\frac{1}{2}+x, \frac{3}{2}-y, \frac{1}{2}+z$; (iv) $-\frac{1}{2}+x, -\frac{1}{2}+y, z$; (v) $\frac{1}{2}-x, -\frac{1}{2}+y, \frac{1}{2}-z$; (vi) $1-x, 2-y, -z$; (vii) $x, 2-y, -\frac{1}{2}+z$; (viii) $-x, y, \frac{1}{2}-z$; (ix) $-x, 2-y, -z$; (x) $\frac{1}{2}+x, -\frac{1}{2}+y, z$.
Symmetry codes for $Eu_6Mo_{10}O_{39}$: (i) $\frac{3}{2}-x, \frac{3}{2}-y, 1-z$; (ii) $1-x, y, \frac{3}{2}-z$; (iii) $-\frac{1}{2}+x, \frac{1}{2}+y, z$; (iv) $\frac{3}{2}-x, \frac{1}{2}+y, \frac{3}{2}-z$; (v) $-\frac{1}{2}+x, \frac{3}{2}+y, \frac{1}{2}+z$; (vi) $\frac{3}{2}-x, \frac{3}{2}-y, 2-z$; (vii) $\frac{1}{2}+x, \frac{3}{2}-y, \frac{1}{2}+z$; (viii) $1-x, 1-y, 1-z$; (ix) $x, 1-y, \frac{1}{2}+x$; (x) $1-x, 2-y, 2-z$.

900.6vs(sh), 872.6vs, 841.8s, 823.5s, 784.9vs(br), 753.1s, 743.4s, 729.9s, 717.4s, 418.5m cm^{-1}.

A slow cooling (3°C min^{-1}) of the sample yielded completely different products, consisting of β'-$Eu_2(MoO_4)_3$ and unknown phases.

Preparation of $Eu_6Mo_{10}O_{39}$

$Eu_6Mo_{10}O_{39}$ can be obtained under the same conditions as $Eu_4Mo_7O_{27}$ (Fig. 1c), but in lower reproducibility. We established a reproducible synthesis procedure as follows. The firing of a mixture (100 mg) of Eu_2O_3 and MoO_3 in a 2:7 molar ratio at 800°C for 2h yielded an assembly of small crystals of $Eu_6Mo_{10}O_{39}$. Successful crystal growth was achieved by heating the product (20 mg) mixed with $[Eu_2(H_2O)_{12}Mo_8O_{27}]\cdot 6H_2O$ (20 mg) at 800°C for 2h (Fig. 1d). IR spectrum; 968.1m(sh), 929.5s(sh), 910.2s, 875.5vs, 834.1vs, 797.4vs, 779.4vs, 744.4s, 724.1s, 442.6m cm^{-1}.

X-Ray Crystallographic Analyses

The single-crystal X-ray structural analyses were carried out for $Eu_4Mo_7O_{27}$ and $Eu_6Mo_{10}O_{39}$ using a Rigaku RAXIS-RAPID imaging-plate X-ray diffractometer and the structure analysis software package TEXSAN (10). Structures of $Eu_4Mo_7O_{27}$ and $Eu_6Mo_{10}O_{39}$ were solved by SHELXS-86 (11) and SIR92 (12) respectively, and refined with full-matrix least-squares techniques. Numerical absorption corrections were done using SHAPE (13) and NUMABS (14). All atoms were refined anisotropically. The complete measurement conditions and results of the refinements are summarized in Table 1. Atomic coordinates and

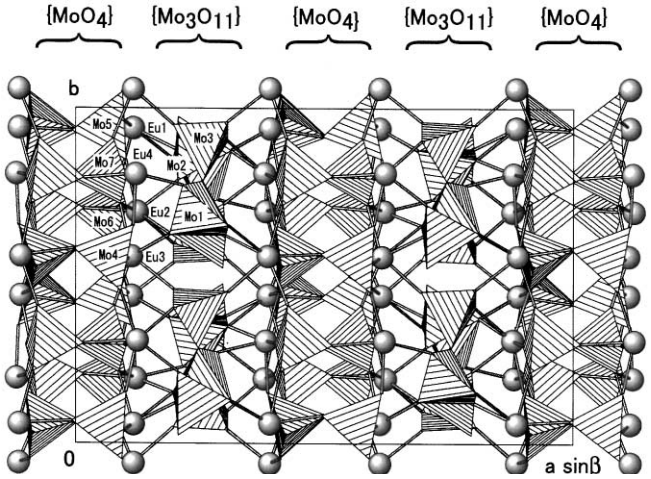

FIG. 2. The structure of $Eu_4Mo_7O_{27}$ viewed down the c axis. The $\{MoO_4\}$ and $\{MoO_5\}$ units are represented polyhedrally. Eu atoms are denoted by gray spheres.

selected bond distances are listed in Tables 2 and 3, respectively. The negative residual difference Fourier peaks were considerably large, 7.2 and -5.8 eÅ^{-3} for $Eu_4Mo_7O_{27}$ and $Eu_6Mo_{10}O_{39}$ respectively, due to poor quality of the single crystals used and/or incomplete absorption correction. Further details of the crystal structure data can be ordered from Fachinformationszentrum Karlsruhe, 76344 Eggenstein-Leopoldshafen (http://www.fiz-karlsruhe.de), under the depository numbers CSD-411960 ($Eu_4Mo_7O_{27}$) and CSD-411961 ($Eu_6Mo_{10}O_{39}$).

Spectroscopies

Contents of Mo and Eu were analyzed by a X-ray fluorescence spectrometer (JEOL JSX-3200). IR spectra were measured by the KBr-disk method on a JASCO FT/IR-410 spectrometer.

RESULTS AND DISCUSSION

Formations of $Eu_4Mo_7O_{27}$ and $Eu_6Mo_{10}O_{39}$

If we assume that the $[Eu_2(H_2O)_{12}Mo_8O_{27}]\cdot 6H_2O$ precursor is completely transformed to $Eu_4Mo_7O_{27}$ or $Eu_6Mo_{10}O_{39}$, the reactions are described as follows.

$$2[Eu_2(H_2O)_{12}Mo_8O_{27}]\cdot 6H_2O \rightarrow Eu_4Mo_7O_{27} + 9MoO_3 + 36H_2O \quad [1]$$

$$3[Eu_2(H_2O)_{12}Mo_8O_{27}]\cdot 6H_2O \rightarrow Eu_6Mo_{10}O_{39} + 14MoO_3 + 54H_2O. \quad [2]$$

The MoO_3 released from the sample recrystallized in the quartz tube of the furnace. The calculated weight losses for the Eqs. [1] and [2] are 53.2 and 54.5%, respectively. However, the main product was the Eu_2O_3–MoO_3 melt, and the observed weight loss was only 36%, indicating that the MoO_3 content in the melt is much larger than those in $Eu_4Mo_7O_{27}$ ($= Eu_2O_3\cdot 3.5\,MoO_3$) and $Eu_6Mo_{10}O_{39}$ ($= Eu_2O_3\cdot 3.33\,MoO_3$). The elemental analysis of the melt showed to have a composition $Eu_2O_3\cdot 6.1MoO_3$. The composition of the melt formed by heating the $Eu_2O_3 + 8MoO_3$ mixture at 800°C was slightly MoO_3-rich ($Eu_2O_3\cdot 6.5MoO_3$). Powder X-ray diffraction patterns revealed that all these melts are amorphous, being in a glass

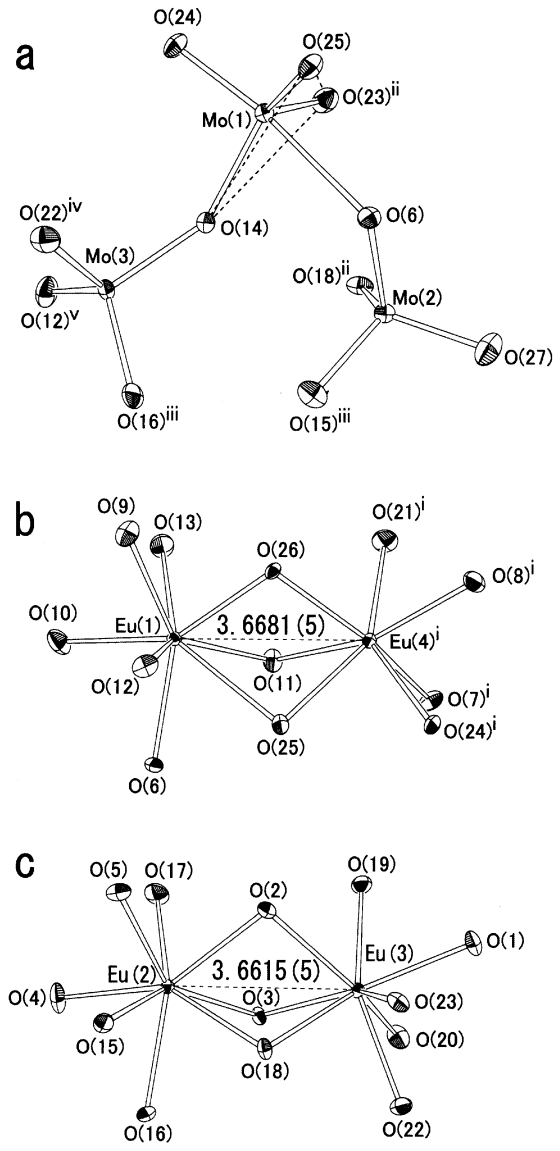

FIG. 3. Views of (a) $\{Mo_3O_{11}\}$, (b) $\{Eu_2O_{12}\}$, and (c) $\{Eu_2O_{13}\}$ groups in $Eu_4Mo_7O_{27}$. The symmetry operations are listed in Table 3.

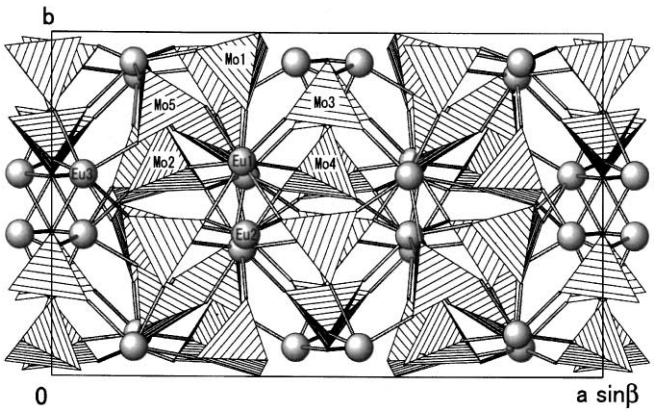

FIG. 4. The structure of $Eu_6Mo_{10}O_{39}$ viewed down the c axis. The $\{MoO_4\}$ units are represented polyhedrally. Eu atoms are denoted by gray spheres.

state after cooling. It should be noted that the IR spectrum of the Eu_2O_3–MoO_3 glass (962m(sh), 962s(sh), 891.9vs(br), 876.5vs(br), 789s(br), 759s(sh) cm^{-1}) is similar to that of stoichiometric compounds $R_2O_3 \cdot 6MoO_3$ (R = La–Gd) (15). Since melting points of the stoichiometric $R_2O_3 \cdot 6MoO_3$ are in the range 680–745°C (15), the amorphous $Eu_2O_3 \cdot 6.1MoO_3$ and $Eu_2O_3 \cdot 6.5MoO_3$ glass phases were formed as a result of the rapid cooling from their liquid states at 800°C.

As described under Experimental, reuse of the same alumina container were effective in enhancing crystallization of $Eu_4Mo_7O_{27}$ and $Eu_6Mo_{10}O_{39}$, suggesting that nucleation occurred gradually on the surface of the container through the repeated exposure to the Eu_2O_3–MoO_3 melt. This is supported by the successful crystal growth of $Eu_4Mo_7O_{27}$ and $Eu_6Mo_{10}O_{39}$ in the Eu_2O_3–MoO_3 melt using the seed-crystal technique (Figs. 1b and 1d). These results indicate that $Eu_4Mo_7O_{27}$ and $Eu_6Mo_{10}O_{39}$ were formed not directly from the decomposition of $[Eu_2(H_2O)_{12}Mo_8O_{27}] \cdot 6H_2O$ (or reaction of $Eu_2O_3 + 8MoO_3$), but via the melt of $Eu_2O_3 \cdot 6.1MoO_3$ (or $Eu_2O_3 \cdot 6.5MoO_3$). On the other hand, the formation of $Eu_6Mo_{10}O_{39}$ by firing the $2Eu_2O_3 + 7MoO_3$ mixture seems to be a direct solid reaction (with loss of MoO_3), because no glassy substance coexisted in the product.

Stoichiometric syntheses excluding the evaporation of MoO_3 have been attempted by the use of evacuated quartz ampoules, in which stoichiometric mixtures of oxides (Eu_2O_3:MoO_3 = 2:7 and 3:10) were heated at 800°C for 2 h. However, no $Eu_4Mo_7O_{27}$ nor $Eu_6Mo_{10}O_{39}$ have been obtained by this procedure. Reaction of $2Eu_2O_3 + 7MoO_3$ at higher temperature (1000°C) in the ampoule gave a mixture of transparent crystals and colored powders. The former compound exhibits an IR spectrum completely different from those of $Eu_4Mo_7O_{27}$ and $Eu_6Mo_{10}O_{39}$. X-ray structural analysis for this product revealed it to be β'-$Eu_2(MoO_4)_3$, which is isostructural with Gd analogue (see Introduction).

Structure of $Eu_4Mo_7O_{27}$

Figure 2 shows the structure of $Eu_4Mo_7O_{27}$ viewed down the c axis. $Eu_4Mo_7O_{27}$ can be best described as a layer compound, consisting of $\{MoO_4\}$- and $\{Mo_3O_{11}\}$-containing layers and interstitial $\{Eu\}$ layers parallel to the bc plane. The $\{Mo_3O_{11}\}$ group is constructed of a distorted $Mo(1)O_5$ trigonal bipyramid and corner-sharing $Mo(2)O_4$ and $Mo(3)O_4$ tetrahedra (Fig. 3a). Such a trimeric molybdate group is the first example among all other structurally characterized rare-earth molybdates where one finds

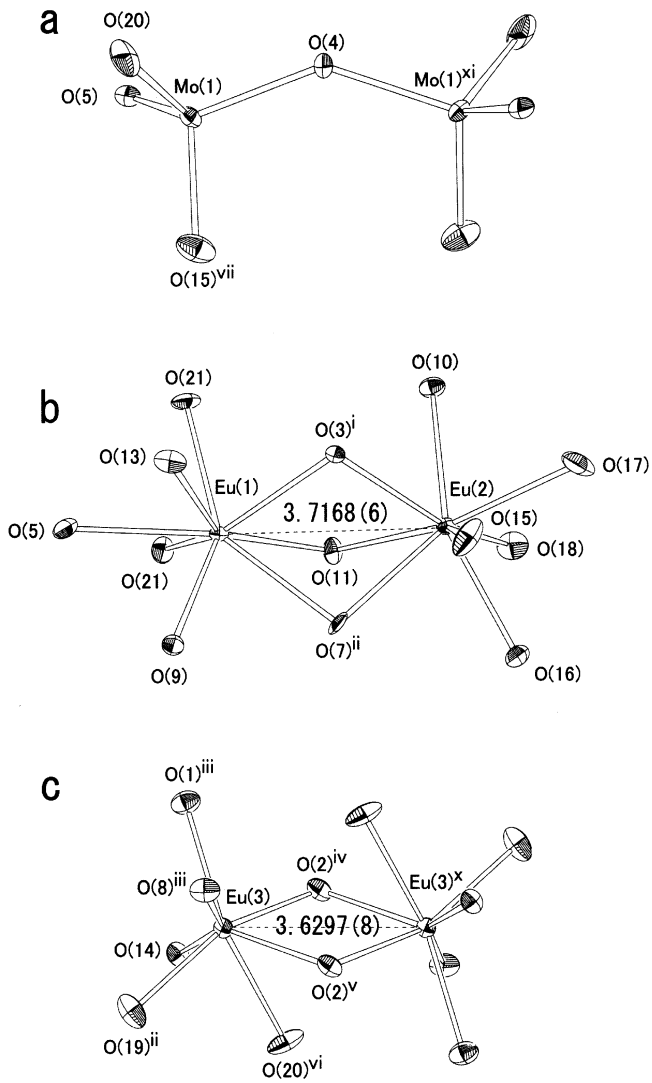

FIG. 5. Views of (a) $\{Mo_2O_7\}$, (b) $\{Eu_2O_{13}\}$, and (c) $\{Eu_2O_{12}\}$ groups in $Eu_6Mo_{10}O_{39}$. The symmetry operations: (xi) $2 - x$, y, $\frac{3}{2} - z$. Other symmetry operations are listed in Table 3.

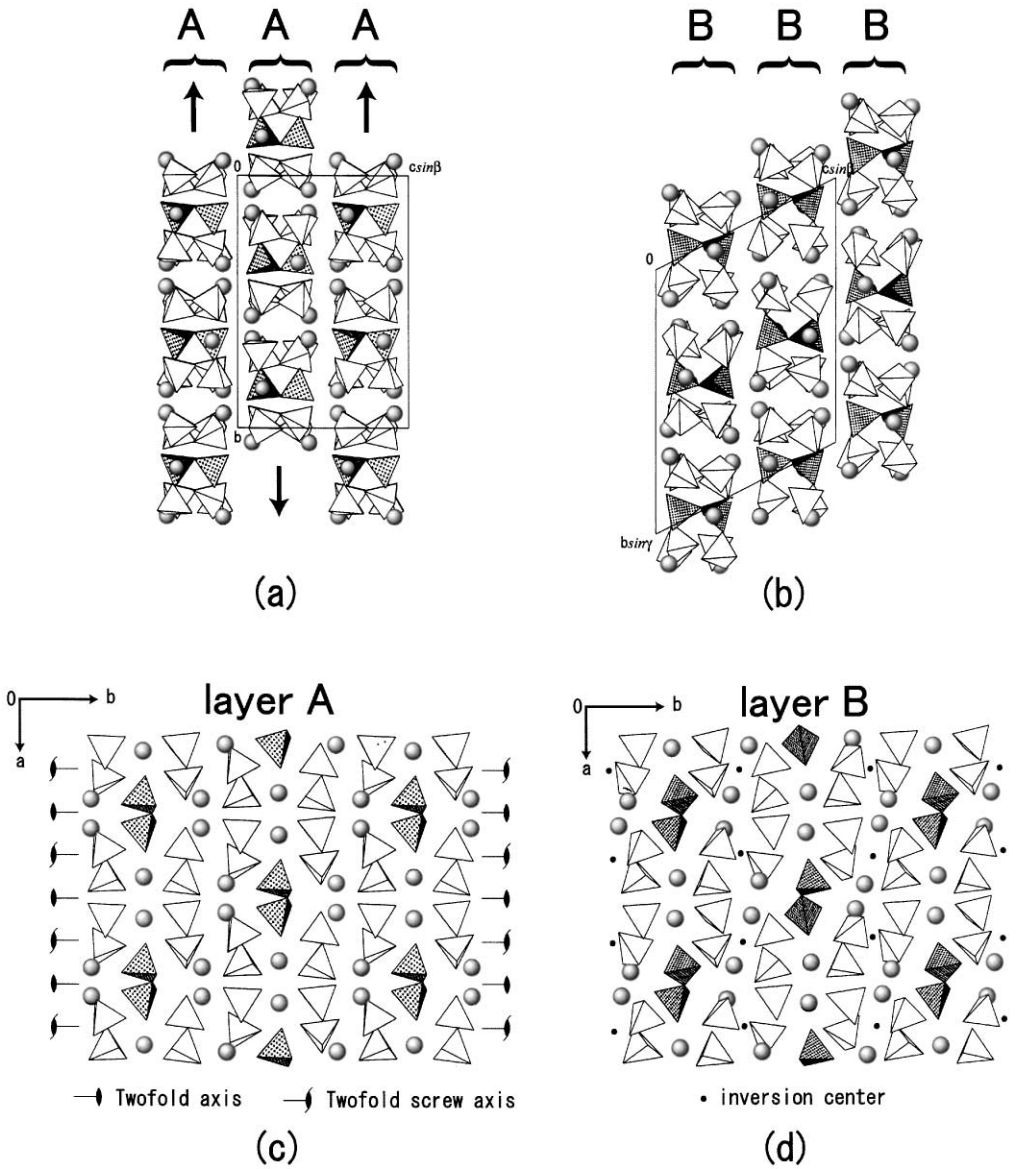

FIG. 6. The structures of (a) $Eu_6Mo_{10}O_{39}$ and (b) $Ce_6Mo_{10}O_{39}$ viewed down the *a* axes. The single layer *A* and *B* projected on to the (001) planes are presented in (c) and (d). The $\{Mo_2O_7\}$ groups are plotted by hatched polyhedra, and Eu and Ce atoms are denoted by gray spheres. The crystallographic twofold and twofold screw axes and inversion centers are also shown in (c) and (d). The arrow in (a) corresponds to the $+b$ direction in (c) (see text).

monomeric $\{MoO_4\}$ in R_2MoO_6 (R = La, Tb) (3) and $La_2(MoO_4)_3$ (16), dimeric $\{Mo_2O_7\}$ in $Ce_6Mo_{10}O_{39}$ (8), tetrameric $\{Mo_4O_{15}\}$ in $Ho_2Mo_4O_{15}$ (17), and polymeric $\{Mo_2O_7\}_\infty$ in $R_2Mo_4O_{15}$ (R = Ce, Pr) (18, 19). The axial Mo(1)–O(6) bond distance (2.368(5) Å) in the $Mo(1)O_5$ polyhedron is much longer than the opposite axial Mo(1)–O(24) bond length (1.726(5) Å). All other Mo(4), Mo(5), Mo(6), and Mo(7) atoms from discrete MoO_4 tetrahedra, which exhibit double $\{MoO_4\}$ layers in the lattice (Fig. 2). Each of the Eu(1), Eu(2), and Eu(3) atoms is surrounded by O atoms (< 2.7 Å) with a distorted square-antiprismatic coordination. These distortions are considerable compared with the nearly ideal square-antiprismatic geometries of the RO_8 sites in polyoxomolybdates, $[R(Mo_8O_{26})_2]^{5-}$ (R = La) (20) and $[R(XMo_{11}O_{39})_2]^{13-}$ (R = Nd, Pr; X = Ge, Si) (21). The Eu(4) atom achieves sevenfold coordination (< 2.7 Å) by O atoms with an approximate monocapped trigonal prism. The $Eu(1)O_8$ and $Eu(4)^iO_7$ polyhedra share the face defined by the O(11), O(25), and O(26) atoms (Fig. 3b). Similarly, the $Eu(2)O_8$ and $Eu(3)O_8$ polyhedra share the face defined by the O(2), O(3), and O(18) atoms (Fig. 3c). These face-sharings of the EuO_n polyhedra result in short $Eu(1)\cdots Eu(4)^i$ (3.6681(5) Å) and $Eu(2)\cdots Eu(3)$ (3.6615(5) Å) separations.

Structure of $Eu_6Mo_{10}O_{39}$ and Comparison with $Ce_6Mo_{10}O_{39}$

Unlike $Eu_4Mo_7O_{27}$, the structure of $Eu_6Mo_{10}O_{39}$ exhibits a three-dimensional network of molybdate groups and Eu atoms. Figure 4 represents a packing diagram of $Eu_6Mo_{10}O_{39}$ viewed down the *c* axis. All of the Mo atoms form MoO_4 tetrahedra, of which $Mo(1)O_4$ is connected with the symmetry-related $Mo(1)^{xi}O_4$ through the O(4) atom, to form a $\{Mo_2O_7\}$ group (Fig. 5a). Other MoO_4 tetrahedra are discrete. Each of the Eu(1) and Eu(2) atoms is square-antiprismatically coordinated by eight O atoms (< 2.7 Å). The $Eu(1)O_8$ and $Eu(2)O_8$ polyhedra are face-shared through the O(11), $O(3)^i$, and O(7) atoms with a short (3.7168 Å) Eu(1)···Eu(2) separation (Fig. 5b). Seven O atoms coordinate to the Eu(3) atom (< 2.7 Å), to give a $Eu(3)O_7$ polyhedron. The $Eu(3)O_7$ and symmetry-related $Eu(3)^xO_7$ polyhedra share the $O(2)^{iv}\cdots O(2)^v$ edge with a short (3.6297(8) Å) $Eu(3)\cdots Eu(3)^x$ separation (Fig. 5c).

The structure of $Eu_6Mo_{10}O_{39}$ is closely related to the previously reported $Ce_6Mo_{10}O_{39}$ (8). The two compounds, which crystallize in different space groups ($P\bar{1}$ and $C2/c$, respectively), are compared in Fig. 6. For convenience, the original axes of $Ce_6Mo_{10}O_{39}$ have been transformed by the matrix $[a' = -a + c;\ b' = a + b + c;\ c' = -a/2 + b/2 - c/2]$ (new cell constants: $a = 12.428$, $b = 19.73$, $c = 13.998$ Å, $\alpha = 77.7$, $\beta = 85.3$, $\gamma = 88.66^\circ$) to be adjusted to the axes of $Eu_6Mo_{10}O_{39}$. Structures of $Eu_6Mo_{10}O_{39}$ and $Ce_6Mo_{10}O_{39}$ viewed along the *a* axes are shown in Figs. 6a and 6b respectively, where similar layers, denoted by *A* and *B*, are stacked in the *c* direction. Single layers *A* and *B* are compared in Figs. 6c and 6d respectively, where small shifts and/or rotations of the MoO_4 tetrahedra and *R* atoms are observed. The layer *A* possesses crystallographic twofold rotational and twofold screw axes parallel to the *b* axis, while the layer *B* has only inversion centers. Also, the $+b$ and $-b$ directions are unequivalent (anisotropic) for the single layer A ($+b$ was denoted by an arrow in Fig. 6c), but are isotropic for the single layer *B*. The stacking of the layers are also different in the two compounds: the layers *A* are stacked with alternate directions (up and down arrows in Fig. 6a), while the layers *B* are stacked with glinding in the *ab* plane (Fig. 6b). The structural difference between $Eu_6Mo_{10}O_{39}$ and $Ce_6Mo_{10}O_{39}$ may be due to the difference in the ionic radius of Eu^{3+} and Ce^{3+}.

ACKNOWLEDGMENT

This work was supported in part by Grant-in-Aid for Scientific Research (Nos. 10304055 and 1274036) from the Ministry of Education, Science, Sports, and Culture.

REFERENCES

1. L. H. Brixner, J. R. Barkley, and W. Jeitschko, *in* "Handbook on the Physics and Chemistry of Rare Earths" (K. A. Geschneidner, Jr. and L. Eyring, Eds.), Vol. 3, Chap. 30, p 610, North-Holland, Amsterdam, 1979.
2. H. J. Borchardt and P.E. Bierstedt, *Appl. Phys. Lett*. **8,** 50–52 (1966).
3. J. S. Xue, M. R. Antonio, and L. Soderholm, *Chem. Mater*. **7,** 333–340 (1995).
4. P. Lacorre, F. Goutenoire, O. Bohnke, R. Retoux, and Y. Laligant, *Nature* **404,** 856–858 (2000).
5. F. Goutenoire, O, Isnard, R. Retoux, and P. Lacorre, *Chem. Mater*. **12,** 2575–2580 (2000).
6. N. Imanaka, T. Ueda, Y. Okazaki, S. Tamura, and G. Adachi, *Chem. Mater*. **12,** 1910–1913 (2000).
7. "Gmelin Handbuch der Anorganischen Chemie," (Deutschen Chemischen Gesellschaft, Ed.), Vol. B2, Chap. 4, p. 101, Springer-Verlag, Berlin, 1976.
8. B. M. Gatehouse and R. Same, *J. Solid State Chem*. **25,** 115–120 (1978).
9. T. Yamase and H. Naruke, *J. Chem. Soc., Dalton Trans*. 285–292 (1991).
10. Molecular Structure Corporation, TEXSAN, Single Crystal X-ray Crystallographic Analysis Software, MSC, 3200 Research Forest Drive, The Woodlands, TX 77381.
11. G. M. Sheldrick, *in* "Crystallographic Computing 3" (G. M. Sheldrick, C. Kruger, and R. Goddard, Eds.), p. 175, Oxford Univ. Press, Oxford, 1985.
12. A. Altomare, M. C. Burla, M. Camalli, M. Cascarano, C, Giacovazzo, A. Guagliardi, and G. Polidori, *J. Appl. Crystallogr*. **27,** 435 (1994).
13. T. Higashi, SHAPE—Program to obtain crystal shape using CCD camera, Rigaku Corporation, Tokyo (1999).
14. T. Higashi, NUMABS – Numerical absorption correction, Rigaku Corporation, Tokyo (1999).
15. L. Z. Gokhman, G. V. Lysanova, D. A. Dulin, and A. V. Pashkova, *Russ. J. Inorg. Chem*. **19,** 1106–1108 (1974).
16. W. Jeitschko, *Acta Crystallogr. Sect. B* **29,** 2074–2081 (1973).
17. V. A. Efremov, N. N. Davydova, L. Z. Gokhman, A. A. Evdokimov, and V. K. Trunov, *Russ. J. Inorg. Chem*. **33,** 1732–1735 (1988).
18. G. D. Fallon and B. M. Gatehouse, *J. Solid State Chem*. **44,** 156–161 (1982).
19. V. A. Efremov, N. N. Davydova, and V. K. Trunov, *Russ. J. Inorg. Chem*. **33,** 1729–1732 (1988).
20. A. Kitamura, T. Ozeki, and A. Yagasaki, *Inorg. Chem*. **36,** 4275–4279 (1997).
21. Y. Shan, Z. Liu, Z. Jin, and G. Wei, *Acta Chim. Sinica* **50,** 357–364 (1992).